euspen's 23rd International Conference & Exhibition, Copenhagen, DK, June 2023
www.euspen.eu

Numerical analysis of different turbine designs for high-frequency spindles

Andreas Lange[1], Nicolas Altherr [1], Benjamin Kirsch[1], Jan C. Aurich[1]

[1]*Rheinland-Pfälzische Technische Universität Kaiserslautern-Landau; Institute for Manufacturing Technology and Production Systems*

andreas.lange@mv.uni-kl.de

Abstract

High-frequency spindles are often used in micro machining for the manufacture of micro structures. The torque, efficiency, and run-out of these spindles depends not only on the bearing but also on the drive. Due to their precise controllability and high efficiency, electric motors are mainly used to drive these high-frequency spindles. However, high speeds and low run-out accuracies can also be achieved with pneumatic drives. The objective of this paper is to investigate the suitability of pneumatic drives for high-frequency spindles. For this purpose, numerical models of different turbine designs are compared with regard to torque, torque ripple, and efficiency. In addition, the influence of eccentric rotation and eccentric inflow on the lateral and longitudinal forces is analysed. Finally, the use of Laval nozzles for the air supply is investigated.

The results show that the torque is not only dependent on the turbine blades' shape, but also on the deflection angle. For the use in high-frequency spindles, the highest torque is not necessarily achieved with double-semicircular blades (Pelton wheel design). Here, the highest torque was achieved using semicircular blades. The lowest lateral forces are found in the turbine with semicircular blades. Longitudinal forces are only observed for the turbine with semicircular blades. Torque ripple can be completely prevented with a bladeless turbine, but with severe losses in efficiency. The use of Laval nozzles leads to an increase in torque and efficiency, regardless of the blade shape.

Finite Element method (FEM), Micromachining, Simulation, Turbine blade

1. Introduction

Due to the small tool diameters in micro machining, which range from 25 to 1000 µm [1], high spindle speeds are necessary to achieve sufficiently high cutting speeds [2]. To generate these high speeds, both electric motors and pneumatic drives can be used. When selecting the drive concept, maximum power, maximum speed, torque ripple, as well as the size and complexity of the drive are particularly relevant. Pneumatic drives achieve high speeds, while allowing for compact geometries [3]. Further advantages are low heat generation [4] as well as the possibility to be designed in such a way that the flow inlets and outlets do not influence the working area of the tool [5].

Various blade shapes have already been used for pneumatic drives. Based on the Pelton turbine, turbines with double-semicircular blades have been used as drives for micro machining in [3], among others. The Pelton turbine has a high efficiency due to the good redirection of the incoming air flow [6], which is why the highest torque can be expected with this blade shape. Turbines with semicircular blades are often used in dentistry [7, 8]. In micro machining, semicircular turbine blades have been used in [4] and [9], among others.

In preliminary work, we have already compared different turbine blade shapes in terms of their performance and efficiency [10]. The highest torque was achieved with a turbine with double-semicircular blades. Comparisons regarding torque ripple, the influence of an eccentricity, and investigations on the effects of Laval nozzles were not carried out.

This paper investigates and compares the suitability of different pneumatic drives for high-frequency spindles regarding their torque, torque ripple, and efficiency. The effects of a dynamic eccentricity and of Laval nozzles are also investigated.

2. Methods

An overview of the turbine designs is shown in figure 1. The turbine geometries are classified based on their deflection angle α. This is the angle by which the air flow is redirected after impact with the turbine. The modelled geometries are turbines with large, medium, and small deflection angles (167° for designs I and II, 130° for designs III and IV, 90° for design V). For the bladeless turbine (design VI), there is no redirection of air flow. All turbines, except for the bladeless turbine, were designed with six blades and two flow inlets. The length and diameter of the turbines are identical.

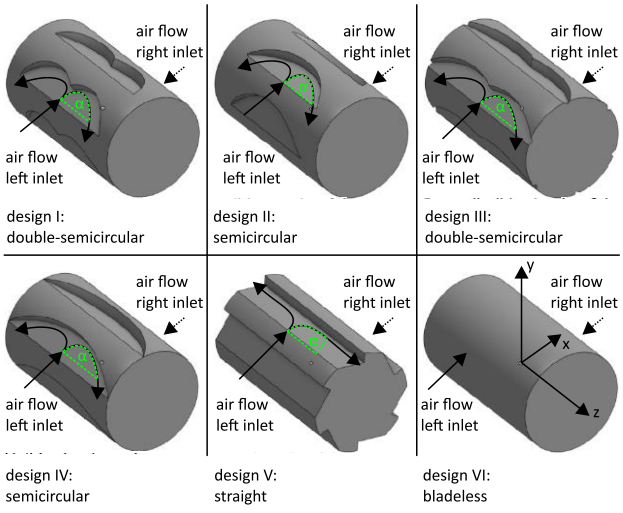

Figure 1. CAD models of the analysed turbine blade designs

The nominal design point for all turbines was targeted to reach a torque of 0.02 Nm at a rotational speed of 150,000 min^{-1}. These numbers are suitable to make comparisons with commercially available (electric motor driven) high frequency spindles.

The same design point is used for all turbines, which is why the mass flow used differs due to the different geometries and deflection angles: 0.0038 kg/s for the turbines with large deflection angles (design I and II), 0.0044 kg/s for the turbines with medium deflection angles (design III and IV) , and 0.0076 kg/s for the turbine with straight blades and the bladeless turbine.

For the simulations, the region in which the fluid is located, i.e., the region between the housing and the turbine, is modelled. This fluid volume is then further subdivided into a static and a rotating fluid zone, to specify a rotating speed for the rotating fluid zone (in this case, the turbine blades) during the simulations. The accuracy of the simulations and the required mesh element size was derived from a mesh independence study.

The energy equation was considered as required for the simulation for compressible fluids. The fluid, in this case air, is modelled as an ideal gas. Further, turbulence is considered. The mass flow rate is specified at each of the flow inlets. In addition, an estimate of the static pressure at the flow inlet is given. This supports the robustness of the computation and leads to a faster convergence of the simulation.

The position of the flow inlets is constant, but the corresponding relative position of the blades changes due to the rotation of the turbine. This results in a changing interaction between the inflowing air and the turbine blades. This leads to torque ripple, which can be determined by simulating different relative positions of the turbine blades.

To model eccentric rotation, the turbine's axis of rotation is moved by 100 µm along the positive x-direction. While bearing gaps used in micro machining are often below 100 µm, this value is well suited to demonstrate and analyse the effects of eccentric rotation lateral forces, while minimizing the influence of modelling errors without requiring excessive refinement of the mesh. The eccentric rotation of the turbine results in a translational motion being applied to the turbine in addition to the rotation. The corresponding equations for the velocities $\dot{x}_s$ and $\dot{y}_s$ and positions x_s and y_s of the centre of gravity can be written as follows (ε: eccentricity, Ω: angular velocity, φ: rotational angle):

$$\dot{x}_s = \varepsilon \cdot \Omega \cdot \sin(\varphi)\,; x_s = -\varepsilon \cdot \cos(\varphi) \quad (1)$$

$$\dot{y}_s = \varepsilon \cdot \Omega \cdot \cos(\varphi)\,; y_s = \varepsilon \cdot \sin(\varphi) \quad (2)$$

Figure 2(a) shows the positions of the turbine's centre of gravity for one revolution.

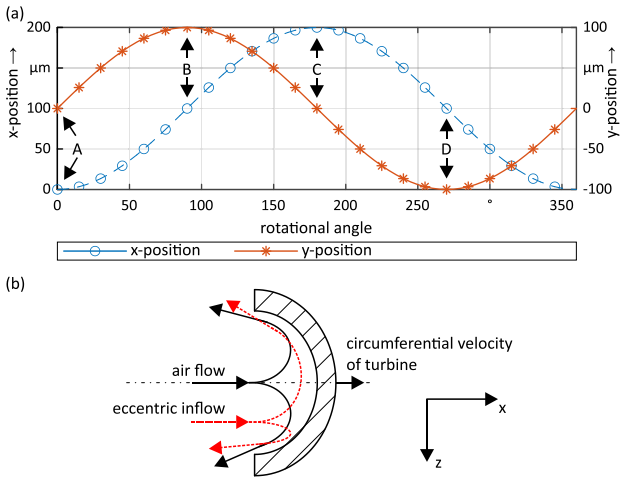

Figure 2. Visualization of eccentric rotation (a) and eccentric inflow (b) of the turbine

To model eccentric rotation, 24 simulations were performed for one revolution of each design, divided into 15°-steps. Each point represents a single step that was simulated. Points of particular interest are marked with letters. At point A, the turbine is not deflected in any direction, but the velocities are non-zero due to eccentricity. At points B, C, and D the turbine is deflected maximally in x-/y-direction.

In addition to the lateral forces caused by an eccentric rotation of the turbine, longitudinal forces in the direction of the axis of rotation (z-axis) are also investigated. Longitudinal forces are caused by an off-centre inflow of the turbine as can be seen in figure 2(b). Longitudinal forces can only be observed for the turbine with semicircular blades. All other geometries redirect the incoming air in such a way that eccentric inflow does not generate longitudinal forces. For modelling purposes, the inlets and outlets were moved along the z-axis by 100 µm.

3. Results

As mentioned in section 2, the mass flow rate at the flow inlet was adjusted in such a way that the resulting torque in the nominal design point is equal for each turbine geometry. Therefore, the transferred torque and transferred force is divided by this mass flow rate to be able to compare the turbines with each other. The results of this division are referred to as relative torque and relative force. The associated units of measurement are Nm/kg/s, i.e., the transmitted torque per kilogram of inflowing fluid and N/kg/s, i.e., the transmitted torque per kilogram of inflowing fluid.

3.1. Comparison of different turbine blade shape designs

Figure 3 shows the relative torques for the different turbine geometries. It should be noted that the negative relative torque for the bladeless turbine is a result of the simulation method used, where a rotational speed is specified as a boundary condition. A computed negative relative torque means that the turbine is not capable of achieving this rotational speed in reality.

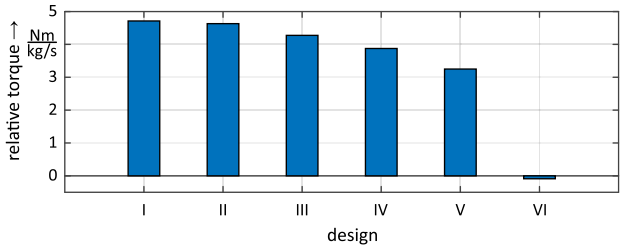

Figure 3. Generated relative torque of all turbine designs at a rotational speed of 150,000 min^{-1}

Figure 3 shows that the geometries with a smaller deflection angle (see section 2 and figure 1) achieve a lower relative torque (and thus also a lower efficiency) than the geometries with a larger deflection angle. Further, it can be noted that the turbine with the semicircular blade can provide a higher relative torque than the turbine with double-semicircular blades.

To investigate this behaviour in more detail, figure 4 shows the velocity profiles on the semicircular blade and the double-semicircular blade. These profiles show the location on the blade where the largest force is applied.

For the double-semicircular blade, the resulting force F_{res} of the impact can be decomposed into an x- and z-component ($F_{x,res}$ and $F_{z,res}$). However, only the x-component is relevant for the transmission of torque to the turbine. In the case of the semicircular blade, this decomposition of the resulting force is not possible due to the blade geometry, and thus the entire impact

force is used to transmit the torque. Further, the simulation results show that the flow velocity is sometimes significantly higher than the speed of sound.

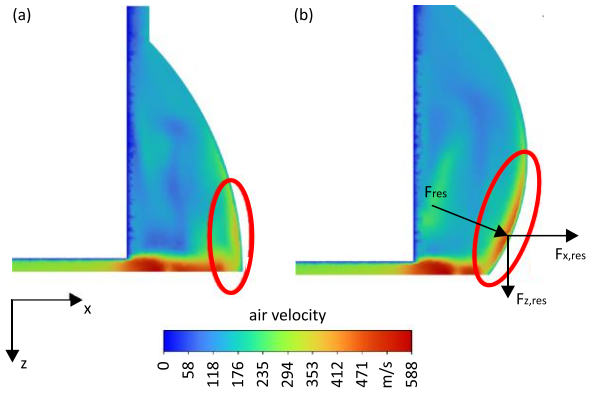

Figure 4. Velocity profiles for the semicircular blade (a) and double-semicircular blade (b)

Figure 5 shows the relative torque curves over one sixth of a revolution for the turbines with semicircular and double-semicircular blades. In general, it can be said that both curves exhibit a sinusoidal pattern. The torque ripple is smaller for the turbine with semicircular blades. The shown torque ripple can be prevented by using a bladeless turbine, but for the investigated geometries, the torque is insufficiently small.

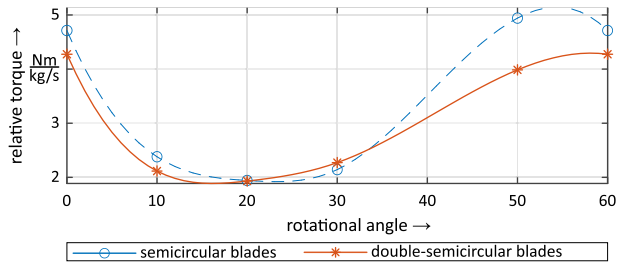

Figure 5. Generated relative torque versus rotational angle for turbines with semicircular and double-semicircular blades at a rotational speed of 150,000 min^{-1}

3.2. Lateral forces due to eccentric rotation

Qualitatively, an oscillating force pattern can be observed for all turbine designs, except for the turbine without blades. For the turbine design without blades, the eccentric motion only leads to a sinusoidally changing force pattern corresponding to the rotational frequency.

Since the oscillating force pattern can be observed for all designs with blades, quantitative results are only shown for the turbine with semicircular blades. For this purpose, figure 6(a) shows the absolute lateral forces for one full revolution at a rotational speed of 150,000 min^{-1}. As can be seen, both forces in x- and y-direction exhibit strongly oscillating behaviour. This is caused by the superposition of the rotational and translational motion due to eccentricity and the constantly changing positions of the blades.

Comparing the force pattern of figure 6(a) with the position of the centre of gravity at the same rotational angle (see figure 2(a)), the following can be stated for the points A, B, C, and D: Due to the eccentric rotation, the translational velocities at point A are not equal to zero, which is why the forces at this point are also not equal to zero, even though the turbine is in the centre of the stator. At point B, the deflection of the turbine in x-direction is equal to half of the maximum deflection. The forces in x-direction are therefore at a high level, but do not yet reach their maximum. The deflection in y-direction is at its highest at this point. However, the maximum force magnitude in y-direction does not coincide with this point. This is once again because in addition to the eccentric motion, the blade positions vary with the angle of rotation. At point C, the force in x-direction reaches its maximum at a rotation angle of approx. 180° to 200°. The angle of rotation at which the forces reach their maximum coincides with point C in figure 2(a). Thus, the lateral forces are at their highest level when the turbine is deflected maximally in x-direction. This is because the gap between the turbine and the right inlet becomes minimal, while it increases at the left inlet. The behaviour of the forces at point D is analogous to that at point B; differences in the force amplitudes result from the different instantaneous position of the blades and the eccentricity being applied in the opposite direction.

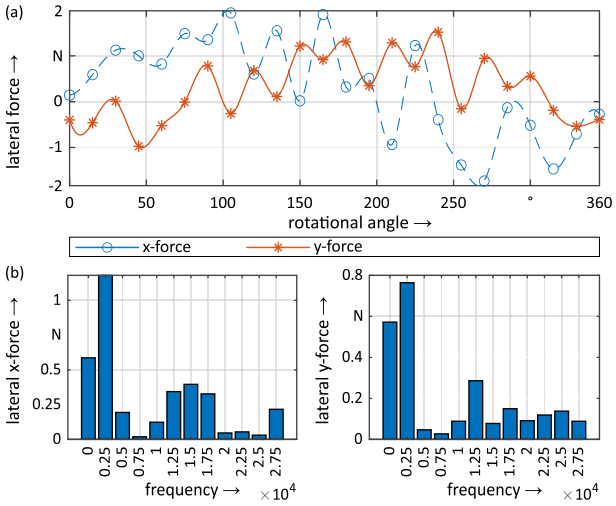

Figure 6. Absolute lateral forces for one full revolution (a) and frequency spectrum (b) of the absolute lateral forces of the turbine with semicircular blades at a rotational speed of 150,000 min^{-1}

Figure 6(b) shows the frequency spectrum of the absolute lateral forces of the turbine with semicircular blades for one full revolution. The highest force amplitudes belong to the frequencies that correspond to the rotational frequency of the turbine (150,000 min^{-1} or 2,500 Hz). The eccentricity and the associated superposition of translational and rotational motion as well as the changing blade positions during one revolution also explain the frequency peaks in the middle and high range, and generally the occurrence of many different frequencies.

For quantitative comparisons of the lateral forces of the different turbine designs, the absolute lateral forces are divided by the mass flow rate. Just like the relative torque, the relative lateral forces are similar for the turbines with semicircular and double-semicircular blades. However, comparing the relative lateral forces of the turbine with semicircular blades to the forces of the other designs reveals significant differences, as evidenced by table 1. Due to the small deflection angle of the turbine with straight blades and no deflection/redirection of the flow in the case of the turbine without blades (see also figure 1), the relative lateral forces are significantly higher.

Table 1. Maximum relative lateral forces in x- and y-direction for turbine designs with different deflection angles at a rotational speed of 150,000 min^{-1}

turbine design	maximum force in x-direction/N	maximum force in y-direction/N
semicircular blades	509.55	398.78
straight blades	1,358.62	517.90
without blades	2,184.58	864.96

3.3. Longitudinal forces due to eccentric inflow

Table 2 lists the longitudinal forces of the turbine with semicircular blades for different rotational speeds. It is noticeable that the absolute values are very low. From this, it can be concluded that the eccentric inflow does not have a significant negative influence on the operation of the turbine.

Table 2. Longitudinal forces due to eccentric inflow of the turbine with semicircular blades for different rotational speeds

rotational speed/min^{-1}	longitudinal force/mN
60,000 min^{-1}	4.25
90,000 min^{-1}	2.78
120,000 min^{-1}	1.78
150,000 min^{-1}	1.52

It appears as if the longitudinal forces decrease with increasing speed. However, one must consider the numerical accuracy of the simulation. The position of the inlets was offset by 100 µm (see also figure 2(b)), which is comparatively little for the given turbine length of 36 mm. For a more detailed consideration of the speed-dependent behaviour of the longitudinal force, a significant mesh refinement or an increase of the eccentricity value is possible.

3.4. Influence of Laval nozzle

The simulation results show that the flow velocity increases significantly to values higher than the speed of sound (343 m/s for an air temperature of 20°C) after exiting the inlet (see figure 4). Hence, it is investigated whether a higher torque can be achieved with a Laval nozzle at the same input power. The resulting change in torque is shown in table 3 for the turbine with semicircular blades. The Laval nozzle offers an improvement regarding the transmitted torque and thus also the efficiency. This improvement in torque can be observed for all geometries, meaning that the use of a Laval nozzle can be recommended, regardless of the turbine blade design.

Table 3. Comparison of torque for convergent nozzle and Laval nozzle (turbine with semicircular blades)

nozzle design	torque/mNm	ratio
convergent	17,91	-
Laval	25,33	1,41

4. Conclusion and outlook

This paper investigated the suitability of pneumatic drives for high-frequency spindles. For this purpose, numerical models of different turbine designs were set up. The numerical models were compared regarding their torque, torque ripple, and efficiency. The influence of eccentric rotation and eccentric inflow on the lateral and longitudinal forces was modelled by a superposition of translational and rotational motion. In addition, the use of Laval nozzles was investigated. The following conclusions can be drawn:

- The comparison of different turbine blade shape designs showed that the highest torque is not necessarily achieved with double-semicircular blades. For the investigated geometries, the highest torque is achieved with semicircular blades. This implies that during the design phase, both semicircular and double-semicircular blades (Pelton wheel design) are worth investigating. Due to the finite number of blades, torque ripple is observed. Semicircular blades showed smaller torque ripple than double-semicircular blades.
- Eccentric rotation due to rotor unbalance leads to oscillating lateral forces which can influence spindle accuracy. For the given design parameters, the lowest lateral forces were found in the turbine with semicircular blades.
- Eccentric inflow only leads to longitudinal forces for the turbine with semicircular blade shape. However, the generated longitudinal forces are not significant and hence have no negative effect on spindle accuracy.
- Torque ripple can be eliminated entirely by using a bladeless turbine, but only at a great loss of efficiency.
- For the use in high-frequency spindles, the use of Laval nozzles is recommended due to the higher generated torque and efficiency.

In future works, further optimizations of turbines with semicircular blades and Laval nozzles will be conducted. Additionally, power, efficiency, torque ripple, lateral and longitudinal forces of these optimized turbines will be compared to electric motors to further investigate the feasibility of turbine drives in high-frequency spindles.

Acknowledgement

This research was funded by the Deutsche Forschungsgemeinschaft (DFG, German Research Foundation) – project numbers 491400536 and – 252408385 – IRTG 2057.

References

[1] Gao S, Cheng K, Ding H, Fu H 2016 Multiphysics-based design and analysis of the high-speed aerostatic spindle with application to micro-milling. Proceedings of the Institution of Mechanical Engineers, Part J: Journal of Engineering Tribology **230(7)** 852-871
[2] Chae J, Park S S, Freiheit T 2006 Investigation of micro-cutting operations. International Journal of Machine Tools and Manufacture **46/3-4** 313-332
[3] Jahanmir S, Ren Z, Heshmat H, Tomaszewski M 2010 Design and Evaluation of an ultrahigh speed micro-machining spindle. International Journal of Machining Science and Technology **11/2** 224-243
[4] Li W, Zhou Z X, Huang X M, He Z J, Du Y 2014 Development of a High-Speed and Precision Micro-Spindle for Micro-Cutting. International Journal of Precision Engineering and Manufacturing **15** 2375-2383
[5] Tamura Y, Sawano H, Yoshioka H, Shinno H 2014 A thermally stable aero- static spindle system equipped with self-cooling function. Journal of Advanced Mechanical Design, Systems, and Manufacturing **8/6**
[6] Zhang Z 2016 Pelton Turbines. Springer Cham
[7] Dyson J, Darvell B 1999 Flow and free running speed characterization of dental air turbine handpieces. Journal of dentistry **27** 465-477
[8] Dyson J, Darvell B 1999 Torque, power and efficiency characterization of dental air turbine handpieces. Journal of dentistry **27** 573-586
[9] Sung H 2007 High-Speed Fluid Bearing Micro-Spindles for Meso-Scale Machine Tools (mMTs). Dissertation, Northwestern University, Evanston
[10] Müller C 2019 Kompakte Luftlagerspindeln für die spanende Mikrobearbeitung auf Desktop-Werkzeugmaschinen. Dissertation, Technische Universität Kaiserslautern